Improve the Dynamic Stability of an Integrated Grid-Connected Offshore Wind Farm and Marine-Current Farm Using FACTS

Jogi Sindhura*, Manda Sridhar**

*(Department of EEE, GIET, JNTU University, Kakinada

** (Department of EEE, GIET, JNTU University, Kakinada

ABSTRACT

This paper presents a control scheme based on Flexible AC Transmission system (FACTS) controller device to achieve both voltage control and damping enhancement of a grid-connected integrated 80-MW offshore wind farm (OWF) and 40-MW marine- current farm (MCF). The performance of the studied OWF is simulated by an equivalent doubly-fed induction generator (DFIG) driven by an equivalent wind turbine (WT) while an equivalent squirrel-cage rotor induction generator (SCIG) driven by an equivalent marine-current turbine (MCT) is employed to simulate the characteristics of the MCF. A damping controller of the STATCOM is designed by using modal control theory to contribute effective damping characteristics to the studied system under different operating conditions. A frequency-domain approach based on a linearized system model using eigenvalue techniques and a time-domain scheme based on a nonlinear system model subject to various disturbances are both employed to simulate the effectiveness of the proposed control scheme. It can be concluded from the simulated results that the proposed STATCOM joined with the designed damping controller is very effective to stabilize the studied system under disturbance conditions. The voltage fluctuations of the AC bus subject to the active-power variations of the studied system can also be effectively controlled by the proposed control scheme.

Keywords − **Dynamic stability, marine-current farm, offshore wind farm, static synchronous compensator.**

I. INTRODUCTION

Currently, both ocean energy and wind energy have been combined together in the United Kingdom [1]–[3]. The ocean is an untapped resource that is capable of making a major contribution to our future energy needs. There are several different forms of ocean energy that are being investigated as potential resources for power generation. Ocean energy includes thermal energy, wave energy, offshore wind energy, tidal energy, ocean current energy, etc.Marine-current turbine generators (MCTGs) combined with offshore wind turbine generators (WTGs) will become a new trend for energy production in the future. There has been an extensive growth and quick development in the exploitation of wind energy in recent years, which requires the development of larger and more robust wind energy conversion systems. Today, more than 28 000 WTGs are successfully operating all over the world. Since oceans are covering more than 70% surface of the earth, a hybrid power generation system with both offshore wind farm (WF) and

marine-current farm (MCF) can be extensively developed in the whole world in the future. One of the simple methods of running a WF or an MCF is to use many induction generators (IGs) connected directly to the power grid because IGs have the inherent advantages of cost effectiveness and robustness for variable-speed energy conversion systems. Moreover, both WTGs and MCTGs have very similar operating characteristics. However, an IG requires reactive power for magnetization. When the generated active power of an IG is varied due to wind or marine-current fluctuations, the absorbed reactive power and the terminal voltage of the IG can be significantly affected. The generated power and the terminal voltage of an IG are always fluctuating with time due to the inherent random characteristics of wind speed and marine-current speed. A power control scheme of a WF or an MCF is required under normal operation to allow proper control over active power production. In the event of increasing grid disturbances (e.g., grid faults), an energy storage system for a WF is generally required to compensate fluctuating components generated by the WF. A WF may combine with different flexible ac transmission system (FACTS) devices and energy storage systems such as static compensator (STATCOM) [4], [5], etc.

The analyzed results of stability improvement of power systems using STATCOMs and the damping controller design of STATCOMs were presented in [6]. The design of an output feedback linear quadratic controller for a STATCOM and a variable-blade pitch of a wind energy conversion system to perform both voltage control and mechanical power control under grid-connection or islanding conditions were shown in [7]. System modelling and controller design for fast load voltage regulation and mitigation of voltage flicker using a STATCOM were demonstrated in [8]. A new D-STATCOM control algorithm enabling separate control of positive- and negative-sequence currents was proposed, and the algorithm was based on the developed mathematical model in the coordinates for a D-STATCOM operating under unbalanced conditions [9]. An in-depth investigation of the dynamic performance of a STATCOM and a static synchronous series compensator (SSSC) using digital simulations was performed in [10]. The results of a study on the application of the recently developed STATCOM for the damping of torsional oscillations occurred in a series compensated AC system

were studied while dynamic performance of the nonlinear system with an optimized STATCOM controller was evaluated under a three-phase fault condition [11]. Discussion and comparison of different control techniques such as PSS, static VAR compensator (SVC) and STATCOM for damping undesirable interarea oscillations in power systems were carried out in [12]. The conventional method of PI control for a STATCOM was compared and contrasted with various feedback control strategies, and a linear optimal control based on LQR control was shown to be superior in terms of response profile and control effort required [13]. A STATCOM based on a current-source inverter (CSI) was proposed, and the nonlinear model of the CSI was modified to be a linear model through a novel modelling technique [14]. The integrated STATCOM/BESS was introduced for the improvement of dynamic and transient stability and transmission capability.

The performance of the different FACTS/BESS combinations was compared and provided experimental verification of the proposed controls on a scaled STATCOM/BESS system [15]. A dynamic voltage control scheme based on a combination of SVC and STATCOM technology on a connected transmission system with IGs in a wind farm was discussed [16]. This paper is organized as below. The configuration and the employed models for the studied integrated OWF and MCF with STATCOM are introduced first. Then, the design procedure and design results for the PID damping controller of the proposed STATCOM using pole-placement technique are depicted. Both steady-state operation points under various wind speeds and marine- current speeds and the comparative dynamic responses of the studied system with and without the designed PID damping controller under a noise wind-speed disturbance, a marine-current speed disturbance, and a three-phase short-circuit fault at the grid are described later. Finally, specific important conclusions of this paper are drawn.

II. MODELS OF THE STUDIED INTEGRATED OWF AND MCF

Fig. 1 shows the configuration of the studied integrated DFIG-based OWF and SCIG-based MCF with the proposed STATCOM. The 80-MW OWF is represented by a large equivalent aggregated DFIG driven by an equivalent aggregated variable-speed WT through an equivalent aggregated gearbox. The 40-MW MCF is represented by a large equivalent aggregated SCIG driven by an equivalent aggregated variable-speed MCT through an equivalent aggregated gearbox. The OWF, the MCF, the STATCOM and a local load are connected to an AC bus that is fed to the onshore power grid through an offshore step-up transformer and undersea cables. The employed mathematical models of the studied system are described as below.

A. Wind Turbine

The mechanical power (in W) produced by a WT can be expressed by

$$P_{\mathrm{mw}} = \frac{1}{2}\rho_w \cdot A_{\mathrm{rw}} \cdot V_W^3 \cdot C_{\mathrm{pw}}(\lambda_w, \beta_w) \qquad (1)$$

Where ρ is the air density in kilograms per cubic meter ($\rho = 1.225$), A_r is the blade impact area in square meters, V_w is the wind velocity in meters per second, C_{pw} is the power

Coefficient of the WT. λ_w is the tip speed ratio of WT, β_w is blade pitch angle of WT in degrees. The wind speed is modelled as the algebraic sum of a base wind speed, a gust wind speed, a ramp wind speed, and a noise wind speed. The detailed equations for these four wind speed components can be referred to [17] while the power coefficient of the WT is given by [18].

The cut-in, rated, and cut-out wind speeds of the studied WT are 4, 15, and 24 m/s, respectively. When V_w is lower than the rated wind speed of the WT (V_{wrated}), $\beta_w = 0^0$. When $V_w > V_{wrated}$, the pitch-angle control system of the WT shown in Fig. 2 activates and the pitch angle of the WT (β_w) increases. Fig. 3 shows the characteristics of the captured per-unit mechanical power versus the per-unit generator rotor speed of one of the forty 2-MW WTs of the studied 80-MW OWF from cut-in wind speed to rated wind speed [19]. The optimal output points in Fig. 3 are the ideal maximum output mechanical power of the WT.
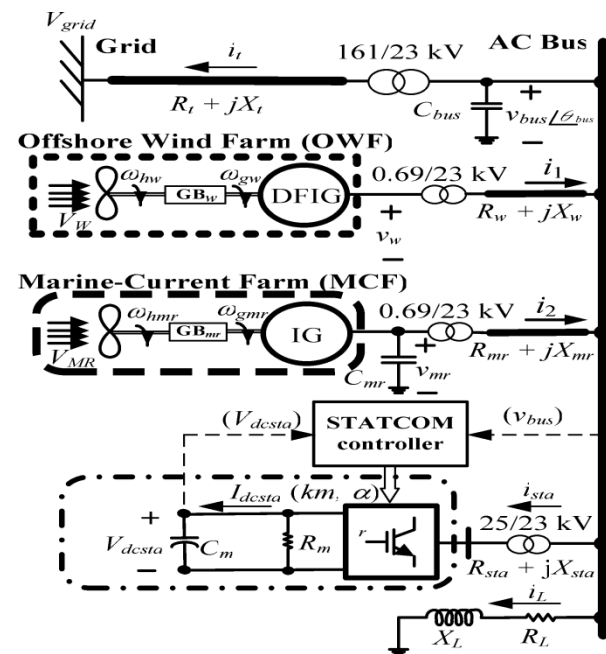

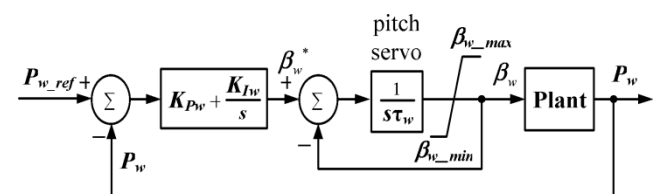Fig.1. Configuration of the integrated OWF and MCF with STATCOM.

Fig.2.Block diagram of the pitch-angle control system of the studied WT.
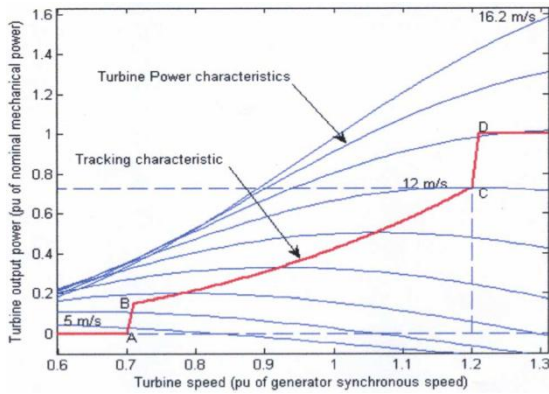
Fig. 3. Characteristics of turbine power versus generator rotor speed [19].
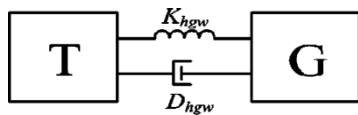
B. Mass-Spring-Damper System and Induction Generator

Fig.4. Two-inertia reduced-order equivalent mass-spring-damper model of the WT coupled to the rotor shaft of the studied wind DFIG.

Fig. 4 shows the two-inertia reduced-order equivalent mass spring-damper model of the WT coupled to the rotor shaft of the studied wind DFIG [20]–[22]. The effect of the equivalent gearbox (GB_w) between the WT and the DFIG has been included in this model. The per-unit - and -axis voltage-current equations of an induction generator can be referred to [25], [26] and they can be used for the electrical parts of the wind DFIG and the marine current SCIG.
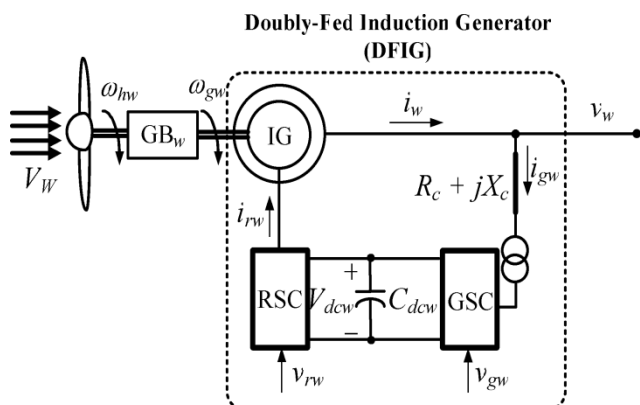
C. Power Converters of DFIG

Fig.5. One-line diagram of the studied doubly-fed induction generator.

Fig. 5 shows the one-line diagram of the studied wind DFIG. The stator windings of the wind DFIG are directly connected to the low-voltage side of the 0.69/23-kV step-up transformer while the rotor windings of the DFIG are connected to the same 0.69-kV side through a rotor-side converter (RSC), a DC link, a grid-side converter (GSC), a step-up transformer, and a connection line. or normal operation of a wind DFIG, the input AC-side voltages of the RSC and the GSC can be effectively controlled to achieve

the aims of simultaneous output active-power and reactive-power control. Fig. 6 shows the control block diagram of the RSC of the studied DFIG. As shown in Fig. 6.
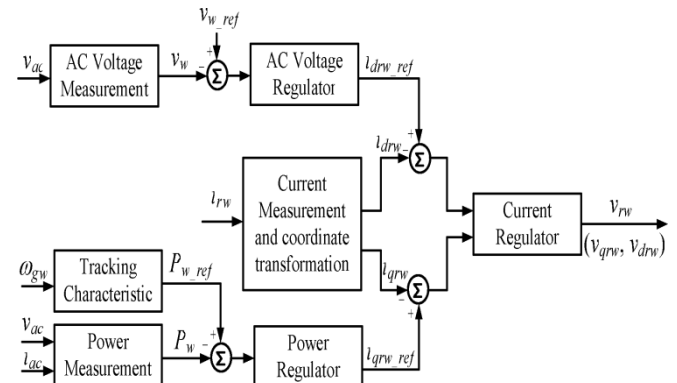

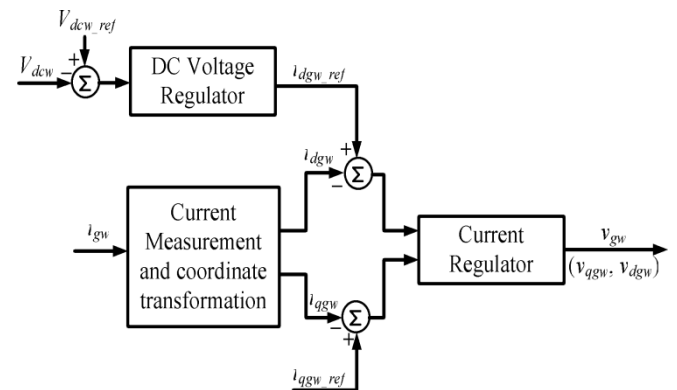Fig. 6. Control block diagram for the RSC of the DFIG.

Fig. 7. Control block diagram for the GSC of the DFIG.

The operation of the RSC requires i_{qrw} and i_{drw} to follow the varying reference points that are determined by maintaining the output active power and the stator-winding voltage at the setting values, respectively. The required voltage for the RSC (v_{rw}) is derived by controlling the per-unit q- and d-axis currents of the RSC [27]–[29]. The control block diagram of the GSC of the studied wind DFIG is shown in Fig. 7. The per-unit - and -axis currents of the GSC, i_{qrw} and i_{drw} have to track the reference points that are determined by maintaining the DC link voltage V_{dcw} at the setting value and keeping the output of the GSC at unity power factor, respectively. The required per-unit voltage of the GSC (v_{gw}) is derived by controlling the per–unit q – and d-axis currents of the GSC [27]–[29].

D. Marine-Current Speed and Marine-Current Turbine

The MCT is assumed to be driven by tide velocities, and the current velocity is determined by spring and neap tides. The marine-current speeds are given at hourly intervals starting at 6 h before high waters and ending 6 h after. It is easy to derive a simple and practical model for marine-current speeds under the knowing tide coefficients as follows:

$$V_{MR} = V_{nt} + \frac{(C_{mr} - 45)(V_{st} - V_{nt})}{95 - 45} \qquad (2)$$

Where C_{mr} is the marine coefficient, 95 and 45 are the

spring and neap tide medium coefficients, respectively, and V_{st} and V_{nt} are the spring and neap marine-current speeds, respectively [1], [3]. The employed marine-current model is between France to England area [1], [3]. The mechanical power (in W) generated by the studied MCT can be expressed by

$$P_{mmr} = \frac{1}{2}\rho_{mr} \cdot A_{rmr} \cdot V_{MR}^3 \cdot C_{pmr}(\lambda_{mr}, \beta_{mr}) \qquad (3)$$

Where ρ_{mr} is the seawater density in kg/m (ρ_{mr} = 1025 kg/m^3), A_{rmr} is the blade impact area in m^2, V_{MR} is the marine velocity in m/s as depicted in (2), and C_{pmr} is the power coefficient of the MCT.

The cut-in, rated, and cut-out speeds of the studied MCT are 1, 2.5, and 4 m/s, respectively. When V_{MR} is higher than the rated speed, the pitch-angle control system of the MCT activates to limit the output power of the MCT at the rated value. Since the employed turbine model, pitch-angle control system, and mass-spring-damper model of the studied MCF are similar to the ones that are employed in the OWF, some mathematical models employed in the OWF can be slightly modified to be used in the MCF except the parameters.

E. STATCOM

The one-line diagram of the studied STATCOM was shown in Fig. 1. The per-unit q- and d-axis output voltages of STATCOM can be expressed by, respectively, [13]

$$v_{qsta} = V_{dcsta} \cdot km \cdot \cos(\theta_{bus} + \alpha) \qquad (4)$$
$$v_{dsta} = V_{dcsta} \cdot km \cdot \sin(\theta_{bus} + \alpha) \qquad (5)$$

Where V_{qsta} and V_{dsta} are the per-unit q- and d –axis voltages at the output terminals of the STATCOM, respectively, θ_{bus} is the phase angle of the AC-bus voltage, V_{dcsta} is the per-unit DC voltage of the DC capacitor C_m, and km and α are the modulation index and phase angle of the STATCOM, respectively. The per-unit DC voltage-current equation of the DC equivalent capacitance C_m can be written as

$$(C_m)p(V_{dcsta}) = \omega_b[I_{dcsta} - (V_{dcsta}/R_m)] \qquad (6)$$

Where

$$I_{dcsta} = i_{qsta} \cdot km \cdot \cos(\theta_{bus} + \alpha)$$
$$+ i_{dsta} \cdot km \cdot \sin(\theta_{bus} + \alpha) \qquad (7)$$

is the per-unit DC current flowing into the positive terminal of V_{dcsta} , R_m is the per-unit equivalent resistance that considers the equivalent electrical losses of the STATCOM, and i_{qsta} and i_{dsta} are the per-unit q- and d -axis currents flowing into the terminals of the STATCOM, respectively. The control block diagram of the proposed STATCOM including a PID damping controller is shown in Fig. 8. The per-unit DC voltage V_{dcsta} controlled by the phase angle α while the voltage V_{sta} is varied by changing the modulation index km. The employed parameters of this paper are listed in Table I.

III. DESIGN OF A PID DAMPING CONTROLLER FOR STATCOM USING MODAL CONTROL THEORY

This section presents a unified approach based on modal control theory to design the PID damping controller of the proposed STATCOM shown in Fig. 8 for dynamic stability improvement of the studied system.
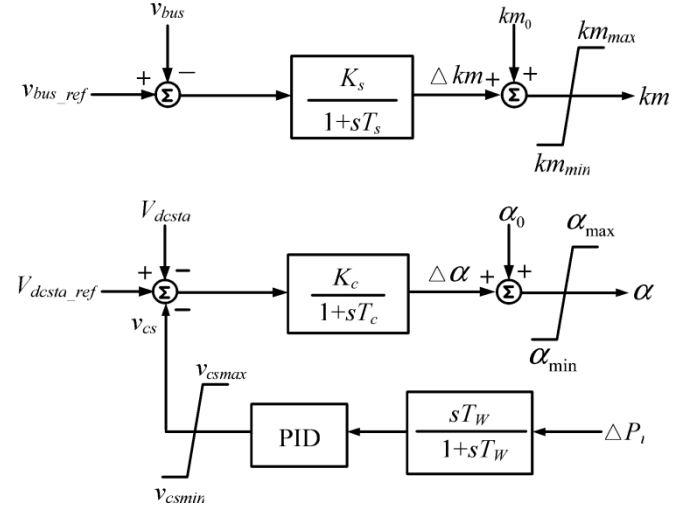

Fig. 8. Control block diagram of the proposed STATCOM including the designed PID damping controller.

TABLE I
EMPLOYED SYSTEM PARAMETERS

System bases
V_{base} = 690 V, S_{base} = 2 MW, ω_{base} = $2\pi f_{bases}$, f_{base} = 60 Hz
Single WT-DFIG of the studied 80-MW OWF
r_{sw} = 0.00706 pu, X_{sw} = 0.171 pu, r_{rw} = 0.005 pu X_{rw} = 0.156 pu, X_{mw} = 2.9 pu, C_{dcw} = 1.0 pu H_{gw} = 0.5 pu, H_{hw} = 2.5 pu, K_{hgw} = 0.3 pu, D_{hgw} = 0.05 pu K_{Pw} = 10.2, K_{Iw} = 30.0, τ_w = 100 s, $\beta_{w\ min}$ = 0°, $\beta_{w\ max}$ = 30°
Single MCT-SCIG of the studied 40-MW MCF
r_{smr} = 0.00488 pu, X_{smr} = 0.09241 pu, r_{rmr} = 0.00549 pu X_{rmr} = 0.09955 pu, X_{mmr} = 3.95279 pu H_{gmr} = 0.5 pu, H_{hmr} = 3.5 pu, K_{hgmr} = 0.1 pu, D_{hgmr} = 0.1 pu K_{Pmr} = 20.0, K_{lmr} = 30.0, τ_{mr} = 120 s, $\beta_{mr\ min}$ = 0°, $\beta_{mr\ max}$ = 30°
STATCOM (±32 MVAR)
R_m = 500 pu, C_m = 0.074 F R_{sta} = 0.05 pu, X_{sta} = 0.2 pu, T_s = 0.01 s, K_s = 0.1 T_c = 0.01 s, K_c = 0.5, km_{max} = 1.0, km_{min} = 0.0, km_0 = 0.5 α_{max} = 45°, α_{min} = -45°, α_0 = 0°, v_{csmax} = 0.2, v_{csmin} = -0.2
Transmission lines, capacitor banks, and local load
R_w = 0.02 pu, X_w = 0.4 pu R_{mr} = 0.02 pu, X_{mr} = 0.4 pu, C_{mr} = 0.3125 pu R_t = 0.04 pu, X_t = 0.8 pu, C_{bus} = 0.125 pu, R_L = 8.0 pu, X_L = 4.0 pu
Constants of power coefficients of WT and MCT
c_1 = 0.34, c_2 =128, c_3 = 0.4, c_4 = c_5 = 0, c_6 = 11 c_7 = 10.9, c_8 = 0.08, c_9 = 0.01 d_1 = 0.18, d_2 =85, d_3 = 0.38, d_4 = 0.25, d_5 = 0.5, d_6 = 10.2 d_7 = 6.2, d_8 = 0.025, d_9 = -0.0443

The nonlinear system equations developed in Section II are first linearized around a nominal operating point to obtain a set of linearized system equations in matrix form of [30]

$$pX = AX + BU + VW \qquad (8)$$
$$Y = CX + DU \qquad (9)$$

Where X is the state vector, Y is the output vector, U is the external or compensated input vector, W is the disturbance input vector while A, B, C and D are all constant matrices of appropriate dimensions. To design a damping controller for the proposed STATCOM, the disturbance input vector W in (8) and the external input vector U in (9) can be properly neglected by letting $D = V = 0$. The state vector X can be partitioned into five sub state vectors as $X = [\ X_{DFIG},\ X_{SCIG},\ X_{MECH},\ X_{ELEC},\ X_{STA}]^T$, where $X_{DFIG}, X_{SCIG}, X_{MECH}, X_{ELEC},$ and X_{STA} are referred to the system state vectors of the wind DFIG, the marine-current SCIG, the mechanical systems of both WT and MCT, the electrical system including the AC bus, three transmission lines and local load, and the STATCOM, respectively. Because V_W seldom reaches the rated wind speed of 15 m/s and V_{MR} seldom operated above the rated marine-current speed of 2.5 m/s, V_W of 12 m/s and V_{MR} of 2.5 m/s are properly selected as the operating points for designing the PID damping controller of the STATCOM.

The eigenvalues and the corresponding damping ratios of the studied integrated OWF and MCF without and with the STATCOM under $V_W = 12$ m/s and $V_{MR} = 2.5$ m/s are listed in the third and the fourth columns of Table II, respectively. The eigenvalues $\lambda_1 - \lambda_4$ and $\lambda_5 - \lambda_8$ listed in Table II relate to the electrical modes of the studied DFIG and SCIG, respectively. The eigenvalues $\lambda_9 - \lambda_{18}$ and $\lambda_{19} - \lambda_{24}$ listed in Table II refer to the mechanical modes and the electrical modes of the studied system, respectively. The eigenvalues $\lambda_{25} - \lambda_{29}$ refer to the modes of the STATCOM. An examination of the eigenvalues listed in Table II has the following points. 1) The DFIG modes, the SCIG modes, and the electrical modes of the studied system are almost fixed on the complex plane; 2) The damping of both $\lambda_{9,10}$ and $\lambda_{11,12}$ is slightly improved when the STATCOM is connected to the integrated OWF and MCF. The damping of both $\lambda_{9,10}$ and $\lambda_{11,12}$ can be simultaneously improved by the addition of the designed PID damping controller; 3) All system eigenvalues are located on the left half of the complex plane under a fixed wind speed and a fixed marine-current speed.

The control block diagram of the phase angle α of the STATCOM including the PID damping controller was shown in Fig. 8. It is seen that the PID damping controller employs the active-power deviation of the transmission line (ΔP_t) as a feedback signal to generate a damping signal V_{cs} in order that the damping characteristics of the poorly damped modes $\lambda_{9,10}$ and $\lambda_{11,12}$ listed in Table II can be effectively improved. Hence, the output signal in (9) is $Y = (\Delta P_t)$ and $U = V_{cs}$ is the input vector. The transfer function $H(s)$ of the proposed PID damping controller in s domain is given by

$$H(s) = \frac{U(s)}{Y(s)} = \frac{v_{cs}(s)}{\Delta P_t(s)}$$
$$= \frac{sT_W}{1 + sT_W}\left(K_P + \frac{K_I}{s} + sK_D \right) \qquad (10)$$

Where T_W is the time constant of the wash-out term while K_P, K_I and K_D are the proportional, integral, and derivative gains of the damping controller, respectively. Taking the Laplace transformation of (8)–(9), an algebraic equation of the closed-loop system containing the PID damping controller can be obtained. The input signal in domain can be expressed by

$$U(s) = H(s)\Delta P_t(s) = H(s)Y(s) = H(s)CX(s). \qquad (11)$$

Combining (10)–(11), we have

$$sX(s) = \{A + B[H(s)C]\}X(s). \qquad (12)$$

The characteristic equation of the closed-loop system including the PID damping controller is given by

$$\det\{sI - [A + BH(s)C]\} = 0. \qquad (13)$$

The four parameters of the PID damping controller can be determined by substituting two pairs of the specified complex-conjugated eigenvalues corresponding to the assigned modes ($\lambda_{9,10}$ and $\lambda_{11,12}$) into (13). The design results of the PID damping controller of the STATCOM are presented as below.

Prespecified Eigenvalues:

$\lambda_{9,10} = -5.5 \pm j4.8$ $\lambda_{11,12} = -15.5 \pm j0.56$.

Parameters of the Designed PID Damping Controller:

$K_P = 10.5$, $K_I = 2.37$, $K_D = 0.06$, $T_w = 0.08$s

The system eigenvalues of the studied integrated OWF and MCF with the proposed STATCOM joined with the designed PID damping controller are listed in the fifth column of Table II. It can be clearly observed that both $\lambda_{9,10}$ and $\lambda_{11,12}$ have been exactly positioned on the desired locations on the complex plane. Some major constraints for selecting the assigned eigenvalues are simply depicted as below [30].

1) The obtained parameters of the PID damping controller should be reasonable. For example, the time constant of the washout term must be positive and the gains of the PID damping controller should be as small as possible.

2) The eigenvalues of the closed-loop system including the designed PID damping controller should be completely located on the left half of the complex plane at the selected operating conditions.

According to the eigenvalue results listed in the fifth column of Table II and the four parameters of the designed PID damping controller of the STATCOM shown above, it can be concluded that both constraints 1) and 2) mentioned above can be simultaneously met.
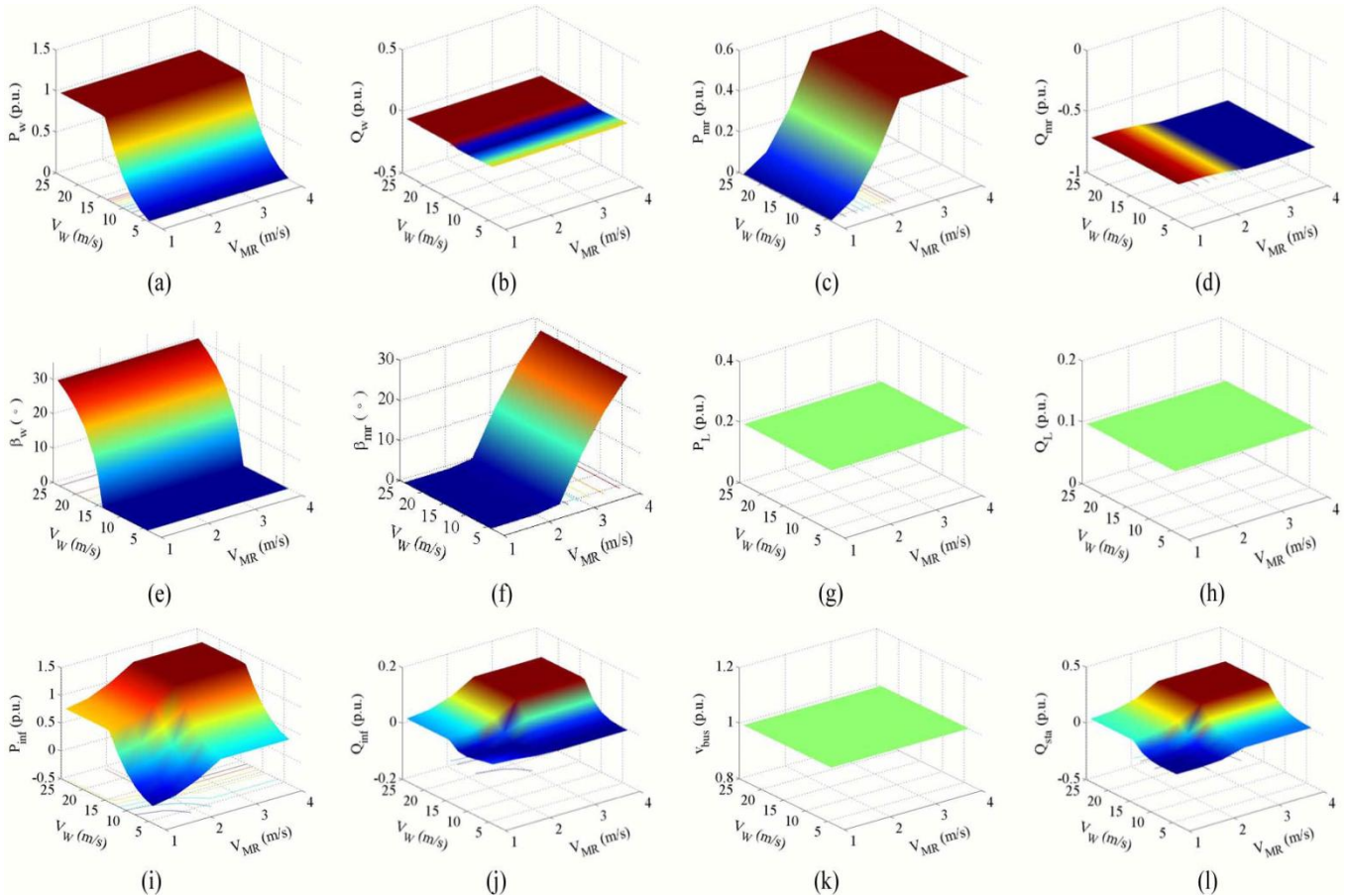
Fig. 9. Steady-state operating conditions of the studied system under various values of wind speed and marine-current speed
(a) P_w, (b) Q_w, (c) P_{mr}, (d) Q_{mr}, (e) β_w, (f) β_{mr}, (g) P_L, (h) Q_L, (i) $Pgrid$, (j) $Qgrid$, (k) V_{bus}, (l) $Qsta$

IV. STEADY-STATE ANALYSIS UNDER VARIOUS OPERATING CONDITIONS

This section presents the steady-state operating condition results of the studied system when V_W is increased from 4 to 24 m/s while V_{MR} is increased from 1 to 4 m/s. Fig. 9 shows thev3-D plots for the calculated steady-state operating conditions of the studied system under the selected values for V_W and V_{MR}. The steady-state operating conditions shown in Fig. 9 are analyzed as below.

1) Fig. 9(a) shows that the output active power of the OWF (P_W) increases with the increase of V_W when V_w is less than the rated wind speed of 15 m/s. Fig. 9(c) shows that the output active power of the MCF (P_{mr}) increases with the increase of V_{MR} when V_{MR} is less than the rated marine current speed of 2.5 m/s.

2) However, the output reactive power of the DFIG-based OWF (Q_w) shown in Fig. 9(b) is kept nearly zero due to the unity-power-factor operation of the GSC of the DFIG. The output reactive power of the MCF (Q_{mr}) shown in Fig. 9(d) is kept a negative constant value due to the inherent required magnetization VAR of the SCIG-based MCF.

3) When P_w or P_{mr} is larger than its rated value, the pitch angle of the WT (β_w) shown in Fig. 9(e) or the pitch angle of the MCT (β_{mr}) shown in Fig. 9(f) increases to limit the output active power at the rated value.

4) The AC-bus voltage magnitude (V_{bus}) shown in Fig. 9(k) can be kept at 1.0 pu by the proposed STATCOM. Hence, the absorbed active power (P_L) and reactive power (Q_L) of the local load can also be kept at constant values as shown in Fig. 9(g) and (h).

5) When both V_W and V_{MR} increase from the cut-in values to the rated values, P_w and P_{mr} increase accordingly and, hence, the active power ($Pgrid$) delivered to the onshore grid increases as shown in Fig. 9(i) but the reactive power ($Qgrid$) delivered to the onshore grid slightly increases as shown in Fig. 9(j). When both V_W and V_{MR} are higher than the rated values, P_w and P_{mr} both $Pgrid$ and $Qgrid$ exhibit flat tops as shown in Fig. 9(i) and (j).

6) The reactive-power variation of the STATCOM ($Qsta$) shown in Fig. 9(l) is similar to the one of $Qgrid$ because $Qsta$ is responsible to supply or absorb the required reactive power from the AC bus to maintain constant V_{bus}.
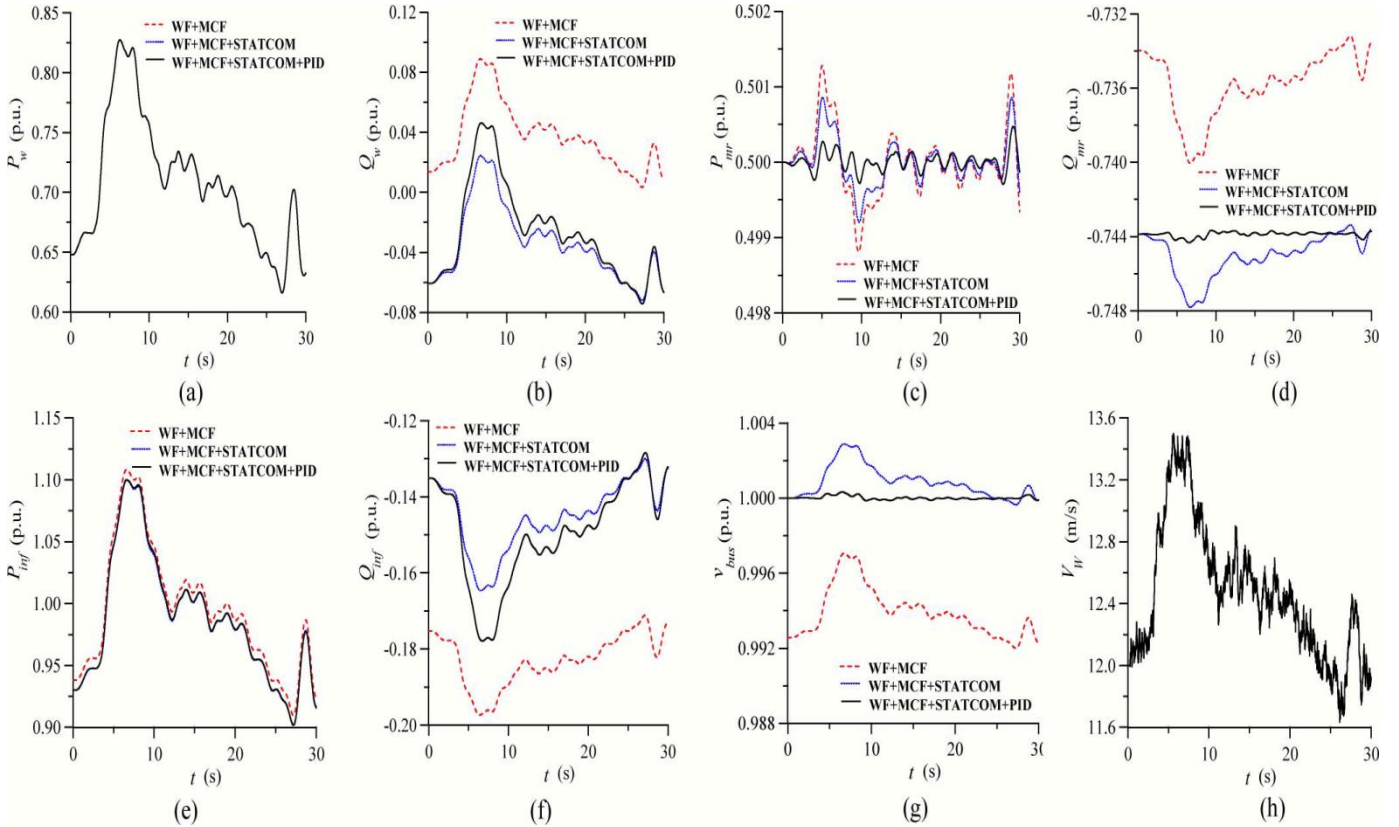
Fig. 10. Dynamic responses of the studied system with and without the designed PID STATCOM damping controller under a noise wind speed disturbance (a)P_w, (b) Q_w, (c) P_{mr} ,(d) Q_{mr}, (e) *Pgrid,* (f) *Qgrid,* (g) V_{bus}, (h) V_w

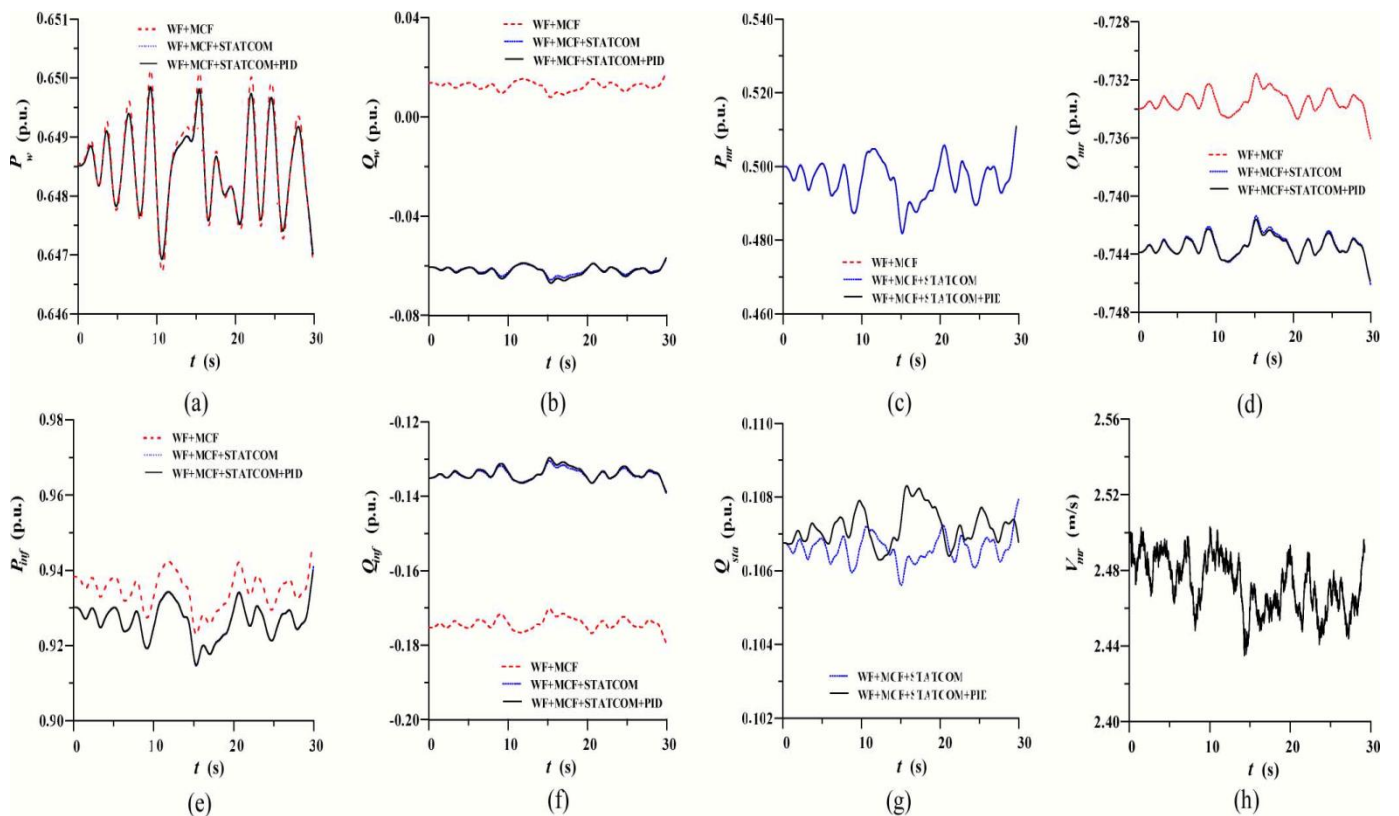

Fig. 11. Dynamic responses of the studied system with and without the PID STATCOM damping controller under a marine-current speed disturbance (a)P_w, (b) Q_w, (c) P_{mr} ,(d) Q_{mr}, (e) *Pgrid,* (f) *Qgrid,* (g) Q_{sta}, (h) V_{MR}
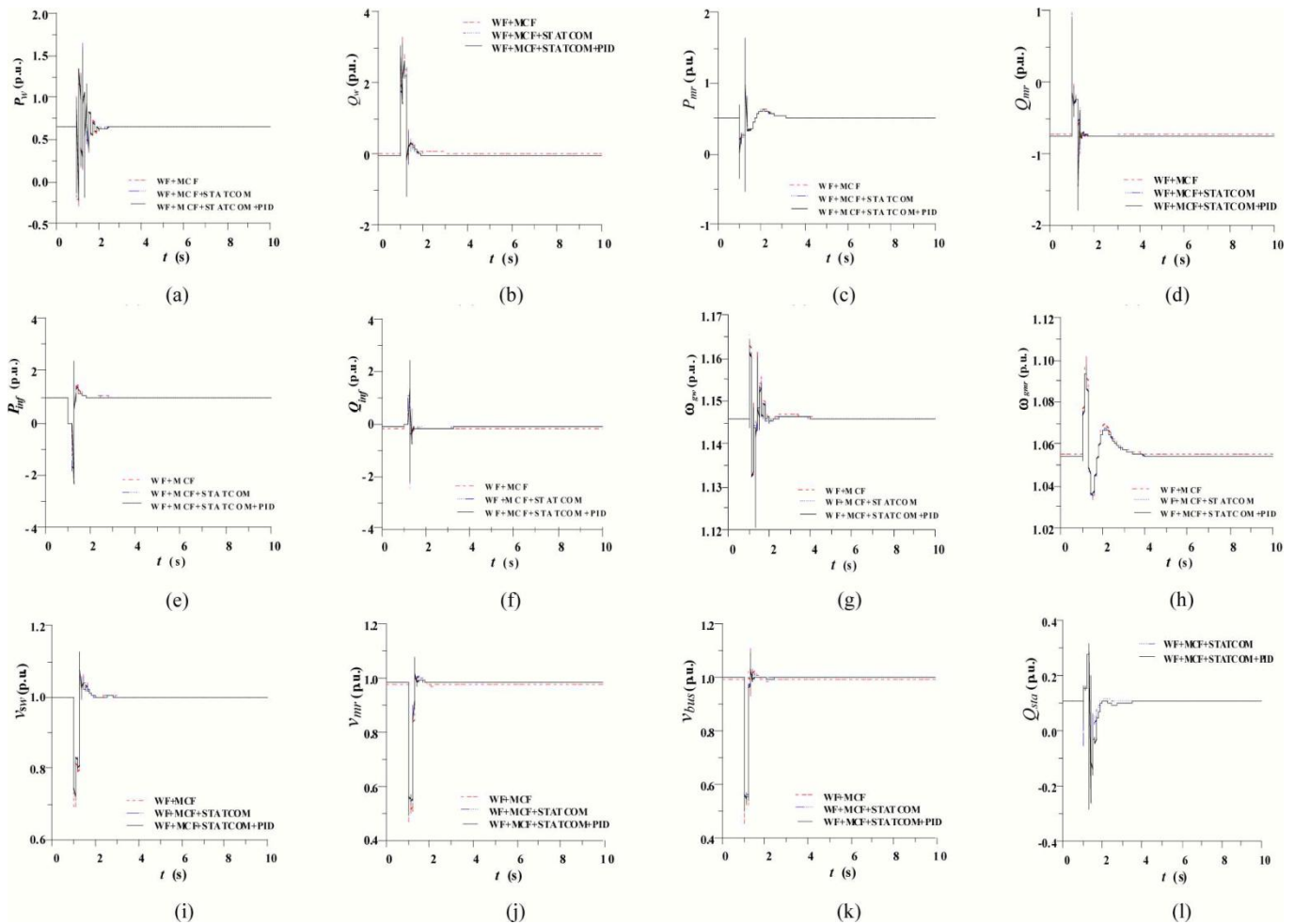
Fig. 12. Transient responses of the studied system with and without the designed PID STATCOM damping controller under a three-phase fault at power grid (a)P_w, (b) Q_w, (c) P_{mr} ,(d) Q_{mr}, (e) *Pgrid,* (f) *Qgrid,(g)* ω_{mr}, (h) ω_{rmr}, (i) V_w, (j) V_{mr}, (k) V_{bus},(l) Q_{sta}

V. NONLINEAR MODEL SIMULATIONS

This section uses the nonlinear system model developed in Section II to compare the damping characteristics contributed by the proposed STATCOM joined with the designed PID damping controller on dynamic stability improvement of the studied system under a noise wind-speed disturbance, a marine-current speed disturbance, and a three-phase short-circuit fault at the grid, respectively.

A. Noise Wind-Speed Disturbance

Fig. 10(a)–(g) illustrates the studied system with and without the proposed STATCOM and the designed PID damping controller under the noise wind-speed disturbance shown in Fig. 10(h). The simulation sequence is as below: 1) When 0 s < t < 0.5 s , the OWF operates under a base wind speed of 12 m/s and the MCF operates under a base marine-current speed of 2.5 m/s; 2) When 0.5 s < t < 30 s , the noise-wind speed shown in Fig. 10(h) is added to the system but the marine- current speed is still kept at V_{MR}=2.5 m/s. The dynamic simulation results shown in Fig. 10(a)–(g) are analyzed as below.

1) It can be seen from the dynamic response of V_{bus} shown Fig. 10(g) that the proposed STATCOM with the designed PID damping controller can

effectively maintain the AC bus voltage at around 1.0 pu by properly adjusting α to tune the quantity of the reactive power of the STATCOM delivered to the AC bus.

2) Because the proposed STATCOM joined with the designed PID damping controller can offer adequate damping characteristics to the studied system, the oscillations of $P_{mr,}$ $\omega_{rmr,}$ V_{mr} and V_{bus} due to the random noise wind speed disturbance can be fast damped, and they have the smallest amplitudes in three curves.

3) The amplitudes of the active power delivered to the power grid (*Pgrid*) shown in Fig. 10(e) and the active power generated by the SCIG of the MCF shown in Fig. 10(c) can be slightly reduced and the absorbed reactive power from the power grid (*Qgrid*) shown in Fig. 10(f) can be decreased when the STATCOM joined with the PID controller is included in the studied system.

4) The generated active power of the DFIG P_w shown in Fig. 10(a) is not affected by the addition of the STATCOM with the PID controller.

B. Marine-Current Speed Disturbance

Fig. 11(a)–(g) plots the studied system with and without the proposed STATCOM and the designed PID damping controller under the marine-current speed disturbance shown in Fig. 11(h). When t < 0 s, the OWF operates under a base wind speed of V_W = 12 m/s and the MCF operates under a base marine-current speed of V_{MR} = 2.5 m/s. It is seen from the dynamic simulation results shown in Fig. 11(a)–(g) that all quantities are slightly deviated from the steady-state operating points at $t = 0$ s due to the small variations on marine-current speed. Since marine-current speed is closely related to the output active power of the MCT, it is seen that the dynamic response of P_{mr} shown in Fig. 11(c) is similar to the one of V_{MR} shown in Fig. 11(h) and the high-frequency components existing in V_{MR} shown in Fig. 11(h) have been filtered out. Comparing the dynamic responses of Q_{mr} shown in Fig. 11(d) with V_{MR} shown in Fig. 11(h), it is found that the magnitude of Q_{mr} gets higher when V_{MR} increases. This is due to the fact that the IG-based MCF requires larger reactive power for magnetization when the rotational speed and the output active power of the SCIG of the MCF increase.

C. Three-Phase Short-Circuit Fault at Power Grid

Fig. 12 plots the transient responses of the studied system with and without the proposed STATCOM joined with the designed PID damping controller under a three-phase short-circuit fault at the grid. The OWF operates under a base wind speed of 12 m/s while the MCF operates under a base marine- current speed of 2.5 m/s. A three-phase short-circuit fault is suddenly applied to the grid at $t = 1$ s and is cleared at $t = 1.25$ s. It is seen from the transient simulation results shown in Fig. 12 that most quantities suddenly drop to low values when the fault occurs. When the fault is cleared, all responses shown in Fig. 12 stably return the original steady-state operating conditions within 4 s. The proposed STATCOM with the designed PID damping controller can offer better damping characteristics to the studied system under the severe three-phase short-circuit fault than without the PID controller.

VI. CONCLUSION

This paper has presented the improvement dynamic stability of an integrated OWF and MCF using a FACTs (STATCOM). A PID damping controller has been designed for the STATCOM by using a unified approach based on pole-assignment approach. Eigenvalue calculations and time-domain simulations of the studied system subject to a noise wind-speed disturbance, a marine- current speed disturbance, and a three-phase short-circuit fault at the grid have been systematically performed to demonstrate the effectiveness of the proposed STATCOM joined with the designed PID damping controller on suppressing voltage fluctuation of the studied system and improving system dynamic stability under different operating conditions. It can be concluded from the simulation results that the proposed STATCOM joined with the designed PID damping controller is capable of improving the performance of the studied integrated OWF and MCF under different operating conditions.

REFERENCES

[1] S. E. B. Elghali, R. Balme, K. L. Saux, M. E. H. Benbouzid, J. F. Charpentier, and F. Hauville, "A simulation model for the evaluation of the electrical power potential harnessed by a marine current turbine," *IEEE J. Ocean. Eng.*, vol. 32, no. 4, pp. 786–797, Oct. 2007.

[2] W. M. J. Batten, A. S. Bahaj, A. F. Molland, and J. R. Chaplin, "Hydrodynamics of marine current turbines," *Renewab. Energy*, vol. 31, no. 2, pp. 249–256, Feb. 2006.

[3] L. Myers and A. S. Bahaj, "Simulated electrical power potential harnessed by marine current turbine arrays in the alderney race," *Renewab. Energy*, vol. 30, no. 11, pp. 1713–1731, Sep. 2005.

[4] H. Chong, A. Q. Huang, M. E. Baran, S. Bhattacharya, W. Litzenberger, L. Anderson, A. L. Johnson, and A. A. Edris, "STATCOM impact study on the integration of a large wind farm into a weak loop power system," *IEEE Trans. Energy Convers.*, vol. 23, no. 1, pp. 226–233, Mar. 2008.

[5] H. Gaztanaga, I. Etxeberria-Otadui, D. Ocnasu, and S. Bacha, "Real-time analysis of the transient response improvement of fixed-speed wind farms by using a reduced-scale STATCOM prototype," *IEEE Trans. Power Syst.*, vol. 22, no. 2, pp. 658–666, May 2007.

[6] K. R. Padiyar and N. Prabhu, "Design and performance evaluation of subsynchronous damping controller with STATCOM," *IEEE Trans. Power Del.*, vol. 21, no. 3, pp. 1398–1405, Jul. 2006.

[7] W. L. Chen and Y. Y. Hsu, "Controller design for an induction generator driven by a variable-speed wind turbine," *IEEE Trans. Energy Convers.*, vol. 21, no. 3, pp. 635–625, Sep. 2006.

[8] A. Jain, K. Joshi, A. Behal, and N. Mohan, "Voltage regulation with STATCOMs: Modeling, control and results," *IEEE Trans. Power Del.*, vol. 21, no. 2, pp. 726–735, Apr. 2006.

[9] B. Blˇazˇic and I. Papic, "Improved D-STATCOM control for operation with unbalanced currents and voltages," *IEEE Trans. Power Del.*, vol. 21, no. 1, pp. 225–233, Jan. 2006.

[10] A. H. Norouzi and A. M. Sharaf, "Two control schemes to enhance the dynamic performance of the STATCOM and SSSC," *IEEE Trans. Power Del.*, vol. 20, no. 1, pp. 435–442, Jan. 2005.

[11] K. V. Patil, J. Senthil, J. Jiang, and R. M. Mathur, "Application of STATCOM for damping torsinal oscillations in series compensated AC system," *IEEE Trans. Energy Convers.*, vol. 13, no. 3, pp. 237–243, Sep. 1998.

[12] N. Mithulananthan, C. A. Canizares, J. Reeve, and G. J. Rogers, "Comparison of PSS, SVC, and STATCOM

controllers for damping power system oscillations," *IEEE Trans. Power Syst.*, vol. 18, no. 2, pp. 786–792, May 2003.

[13] P. Rao, M. L. Crow, and Z. Yang, "STATCOM control for power system voltage control applications," *IEEE Trans. Power Del.*, vol. 15, no. 4, pp. 1311–1317, Oct. 2000.

[14] Y. Ye, M. Kazerani, and V. H. Quintana, "Current-source converter based STATCOM: Modeling and control," *IEEE Trans. Power Del.*, vol. 20, no. 2, pp. 795–800, Apr. 2005.

[15] Z. Yang, C. Shen, L. Zhang, M. L. Crow, and S. Atcitty, "Integration of a STATCOM and battery energy storage," *IEEE Trans. Power Syst.*, vol. 16, no. 2, pp. 254–260, May 2001.

[16] R. Griinbanm, P. Halvarsson, D. Larsson, and P. R. Jones, "Conditioning of power grids serving offshore wind farms based on asynchronous generator," in *Proc. Conf. Power Electronics, Machine and Drives*, Mar./Apr. 2004, vol. 1, pp. 34–39.

[17] P. M. Anderson and A. Bose, "Stability simulation of wind turbine system," *IEEE Trans. Power App. Syst.*, vol. PAS-102, pp. 3791–3795, Dec. 1983.

[18] J. G. Slootweg, H. Polinder, and W. L. Kling, "Representing wind turbine electrical generating systems in fundamental frequency simulations," *IEEE Trans. Energy Convers.*, vol. 18, no. 4, pp. 516–524, Dec. 2003.

[19] L. Wang, T.-H. Yeh, W.-J. Lee, and Z. Chen, "Evaluation of different control strategies on performance of a commercial wind farm," *Int. J. Elect. Eng.*, vol. 16, no. 2, pp. 133–150, Apr. 2009.

[20] D. J. Trudnowski, A. Gentile, J. M. Khan, and E. M. Petritz, "Fixedspeed wind-generator and wind-park modeling for transient stability studies," *IEEE Trans. Power Syst.*, vol. 19, no. 4, pp. 1911–1917, Nov. 2004.

[21] S. M. Muyeen, M. H. Ali, R. Takahashi, T. Murata, J. Tamura, Y. Tomaki, A. Sakahara, and E. Sasano, "Transient stability analysis of wind generator system with the consideration of multi-mass shaft model," in *Proc. Int. Conf. Power Electronics and Drives Systems*, Jan. 16–18, 2006, vol. 1, pp. 511–516. [22] P. Cartwright, L. Holdsworth, J. B. Ekanayake, and N. Jenkins, "Coordinated voltage control strategy for a doubly-fed induction generator (DFIG)-based wind farm," *Proc. Inst. Elect. Eng., Gen., Transm., Distrib.*, vol. 151, no. 4, pp. 495–502, Jul. 2004.

[23] A. G. G. Rodriguez, A. G. Rodriguez, and M. B. Payán, "Estimating wind turbines mechanical constants," in *Proc. Int. Conf. Renewable Energies and Power Quality (ICREPQ'07)*, Vigo, Spain, Mar. 27–30, 2007.

[24] L. Ran, J. R. Bumby, and P. J. Tavner, "Use of turbine inertia for power smoothing of wind turbines with a DFIG," in *Proc. 2004 11th Int. Conf. Harmonics and Quality of Power*, Lake Placid, NY, Sep. 12–15, 2004, pp. 106–111.

[25] Modeling New Forms of Generation and Storage, Jun. 2000, CIGRE, TF.01.10, 5th draft.

[26] P. C. Krause, *Analysis of Electric Machinery*. New York: McGraw-Hill, 1987.

[27] F. M. Hughes, O. Anaya-Lara, N. Jenkins, and G. Strbac, "Control of DFIG-based wind generation for power network support," *IEEE Trans. Power Syst.*, vol. 20, no. 4, pp. 1958–1966, Nov. 2005.

[28] F.Wu, X.-P. Zhang, K. Godfrey, and P. Ju, "Small signal stability analysis and optimal control of a wind turbine with doubly fed induction generator," *IET Gen., Transm., Distrib.*, vol. 1, no. 5, pp. 751–760, Sep. 2007.

[29] M. Kayıkçı and J. V. Milanovic´, "Reactive power control strategies for DFIG-based plants," *IEEE Trans. Energy Convers.*, vol. 22, no. 2, pp. 389–396, Jun. 2007.

[30] L. Wang, S.-S. Chen, W.-J. Lee, and Z. Chen, "Dynamic stability enhancement and power flow control of a hybrid wind and marine-current farm using SMES," *IEEE Trans. Energy Convers.*, vol. 24, no. 3, pp. 626–639, Sep. 2009.

[31] S. M. Muyeen, J. Tamura, and T. Murata, *Stability Augmentation of a Grid-connected Wind Farm*. London, U.K.: Springer-Verlag, Oct. 2008.